The motor activity of myosin-X promotes actin fiber convergence at the cell periphery to initiate filopodia formation

Hiroshi Tokuo,[1] Katsuhide Mabuchi,[2] and Mitsuo Ikebe[1]

[1]Department of Physiology, University of Massachusetts Medical School, Worcester, MA 01655
[2]Muscle Research Group, Boston Biomedical Research Institute, Watertown, MA 02472

Filopodia are actin-rich fingerlike protrusions found at the leading edge of migrating cells and are believed to play a role in directional sensing. Previous studies have shown that myosin-X (myoX) promotes filopodia formation and that this is mediated through its ability to deliver specific cargoes to the cell periphery (Tokuo, H., and M. Ikebe. 2004. *Biochem Biophys. Commun.* 319:214–220; Zhang, H., J.S. Berg, Z. Li, Y. Wang, P. Lang, A.D. Sousa, A. Bhaskar, R.E. Cheney, and S. Stromblad. 2004. *Nat. Cell Biol.* 6:523–531; Bohil, A.B., B.W. Robertson, and R.E. Cheney. 2006. *Proc. Natl. Acad. Sci. USA.* 103:12411–12416; Zhu, X.J., C.Z. Wang, P.G. Dai, Y. Xie, N.N. Song, Y. Liu, Q.S. Du, L. Mei, Y.Q. Ding, and W.C. Xiong. 2007. *Nat. Cell Biol.* 9:184–192). In this study, we show that the motor function of myoX and not the cargo function is critical for initiating filopodia formation. Using a dimer-inducing technique, we find that myoX lacking its cargo-binding tail moves laterally at the leading edge of lamellipodia and induces filopodia in living cells. We conclude that the motor function of the two-headed form of myoX is critical for actin reorganization at the leading edge, leading to filopodia formation.

Introduction

During cell migration, the protrusive leading edge plays a key role in directional movement (Ridley et al., 2003). The leading edge of the migrating cells consists of the two types of actin cytoskeletal architectures, lamellipodia and filopodia. Filopodia is the structure protruding from the edge of the cells that plays an essential role in the wide range of cell motile activities, including cancer cell migration (Wicki et al., 2006; Bennett et al., 2007) and neuronal path finding (Lewis and Bridgman, 1992; Bentley and O'Connor, 1994). Although many studies have been conducted on the role of actin-binding proteins in the actin dynamics at membrane protrusion (Nakagawa et al., 2003; Biyasheva et al., 2004; Lebrand et al., 2004), little is known about the role of the actin-based motor protein myosin in filopodia formation.

Recent studies have revealed that myosin-X (myoX) has an important role in the elongation of filopodia (Berg and Cheney, 2002; Tokuo and Ikebe, 2004; Zhang et al., 2004; Sousa and Cheney, 2005; Bohil et al., 2006; Bennett et al., 2007; Zhu et al., 2007). The N-terminal domain of myoX functions as a motor domain, which is followed by a neck region. The predicted coiled-coil segment is present at the C-terminal side of the neck region (Berg et al., 2000). However, a recent study suggested that this domain does not form a stable coiled coil but instead forms a stable α helix (SAH; Knight et al., 2005). The C-terminal end of the molecule is the tail domain that was reported as a binding portion to the specific cargo molecules (Tokuo and Ikebe, 2004; Weber et al., 2004; Zhang et al., 2004; Zhu et al., 2007). Because myoX moves toward the tip of filopodia and transports the cargo molecules, the function of myoX was thought to simply be that of a cargo carrier.

In this study, we report that the motor activity of myoX is itself critical for the initiation of filopodia formation. Using the inducible dimer-forming technique, we found that dimer formation of myoX without the cargo-binding domain can trigger the initiation of microspikes/filopodia in lamellipodia in living cells. Furthermore, the elimination of myoX abolished the actin bundles and microspikes in lamellipodia, and the dimerized myoX can move laterally at the leading edge of lamellipodia. These findings suggest that the motor activity of myoX plays a role in the convergence of actin fibers in lamellipodia, thus forming the base for the initiation of filopodia.

Correspondence to Mitsuo Ikebe: Mitsuo.Ikebe@umassmed.edu

Abbreviations used in this paper: FKBP, FK506-binding protein; FN, fibronectin; myoV, myosin-Va; myoVII, myosin-VIIa; myoX, myosin-X; SAH, stable α helix; shRNA, small hairpin RNA.

The online version of this article contains supplemental material.

The Journal of Cell Biology, Vol. 179, No. 2, October 22, 2007 229–238
http://www.jcb.org/cgi/doi/10.1083/jcb.200703178

Results and discussion

Dimerization with proper neck length is critical for the filopodial tip localization of myoX

To eliminate the effect of the tail-binding molecules on filopodia formation, we constructed a GFP-tagged tailless myoX (Fig. 1). We produced constructs having the stable two-headed structure because that structure is necessary for continuous movement of the processive myosins (Veigel et al., 2002; Yildiz et al., 2003; Park et al., 2006). We added the coiled-coil domain of myosin-Va (myoV) at the C-terminal end of the SAH domain of myoX (Fig. 1 A, b). GFP signals of this construct showed a distinct localization at the tip of filopodia in COS7 cells (Fig. 1 A, b). Interestingly, the construct lacking the SAH domain (Fig. 1 A, a) failed to show the tip localization, although it formed the two-headed structure. On the other hand, GFP-M10MoIQ3SAH and GFP-M10MoIQ3, having no stable coiled-coil domain, failed to localize at the tip (unpublished data). These results suggest that the formation of the two-headed structure and the presence of the SAH domain are required for the movement of myoX toward the tip of filopodia.

The regulated dimerization system of myoX

To further elucidate the relationship between the dimer formation of myoX and the initiation of filopodia in the living cells, we used the regulated homodimerization system (described in Materials and methods). In the NIH3T3 cells expressing GFP-M10MoIQ3SAH–FK506-binding protein (FKBP), GFP signals were distributed throughout the cell body (Fig. 1 B, a). After the addition of the homodimerizer AP20187, GFP signals became distinctly concentrated at the tip of filopodia (Fig. 1 B, b). In contrast, GFP-M10MoIQ3SAH, having no FKBP domain, did not show the AP20187-induced tip localization (unpublished data). When we used the heterodimerizer AP21967 as a control, GFP-M10MoIQ3SAH-FKBP did not localize at the tip (unpublished data). These results further support the notion that dimer formation is critical for the movement of myoX to the tip of filopodia.

Induction of microspikes/filopodia by dimerization of tailless myoX

To further investigate the potential role of the monomer to dimer transition of myoX in filopodia initiation, we performed quantification of microspikes/filopodia in COS7 cells (Fig. 1 C). The production of microspikes/filopodia of GFP-M10MoIQ3SAH-M5CC was four- to fivefold greater than that of GFP-M10MoIQ3-M5CC (Fig. 1 C). Furthermore, addition of the dimerizer considerably induced the microspike formation in GFP-M10MoIQ3SAH-FKBP–expressed cells, and the number of microspikes was four- to fivefold greater than without dimerizer (Fig. 1 C). These results suggest that the initiation of microspikes/filopodia takes place with the dimer formation of myoX.

Motor function and proper length of the lever arm of myoX

The aforementioned results indicate that three domains (motor, IQ, and SAH) of myoX are essential for the induction of filopodia. It was hypothesized that the motor activity of myoX plays a critical role in the induction of filopodia. To address this idea, we produced the two constructs having motor-dead mutation in switch I (R220A) or switch II (G437A) of GFP-M10MoIQ3SAH-FKBP. These two mutations were found to inhibit both the localization of myoX at the tip of filopodia and the induction of filopodia even after the addition of dimerizer (Fig. 2 A). These results support a critical role for the motor activity of myoX in filopodia formation.

It has been proposed that the SAH domain may function as part of the myoX lever (Knight et al., 2005). To investigate a correlation between the neck length and filopodia formation, we constructed the myoX vectors that have different neck lengths by introducing a different number of IQs from myoV (Fig. 2 B). The introduction of one IQ domain from myoV to the SAH-deleted construct (Fig. 2 B, a) considerably (four- to fivefold) increased the initiation of microspikes, and the expressed molecules were concentrated at the tip of filopodia (unpublished data). There was no difference in the number of microspike/filopodia between the constructs having one or two additional IQs (Fig. 2 C). The addition of even more IQs (M5(456), M5(3456), and M5(23456)) did not further increase the number of microspikes (unpublished data).

It was reported that myosin-VIIa (myoVII) also has a SAH domain in the predicted coiled-coil region (Knight et al., 2005). To investigate whether the function of the SAH domain of myoX (M10SAH) is caused by the specificity of the M10SAH structure, we swapped M10SAH for M7SAH of the original construct (Fig. 2 B, c). The swapped construct induced the microspike/filopodia after the addition of dimerizer, similar to the original construct (Fig. 2 C). It was calculated that the length of the SAH domain used in this study was ∼5.4 nm, and one IQ domain was 3.5 nm (Knight et al., 2005). Based on this calculation, the lengths of three IQs and a SAH (Fig. 1 A, b), four IQs without the SAH (Fig. 2 B, a), and five IQs without the SAH (Fig. 2 B, b) were 15.9 nm, 14.0 nm, and 17.5 nm, respectively. These results suggest that deletion of the SAH hampered the proper movement of myoX because of the lack of sufficient neck length. The results also indicate that it is important for myoX movement to have the certain minimum neck length. Therefore, it is likely that the SAH domain provides enough span and flexibility for myoX heads to search for the proper binding sites on actin filaments.

Dimerizer-induced formation of the two-headed structure of myoX

To examine whether AP20187 actually induces dimer formation in the cells, we expressed myc-M10MoIQ3SAH-FKBP along with GFP-M10MoIQ3SAH-FKBP-HA in COS7 cells (Fig. 3 A). The cells cotransfected with the aforementioned two constructs were incubated with or without AP20187. The myoX construct immunoprecipitated with anti-HA antibodies was recognized by both anti-myc and anti-HA antibodies only when the cells were incubated with AP20187 (Fig. 3 B, lane 4). The result indicates that AP20187 induces the dimer formation of M10MoIQ3SAH-FKBP in cells. It should be noted that the dimer formation of the same construct was not detected with AP21967 (unpublished data). To directly visualize the structure of the molecules of the myoX constructs, the isolated myoX

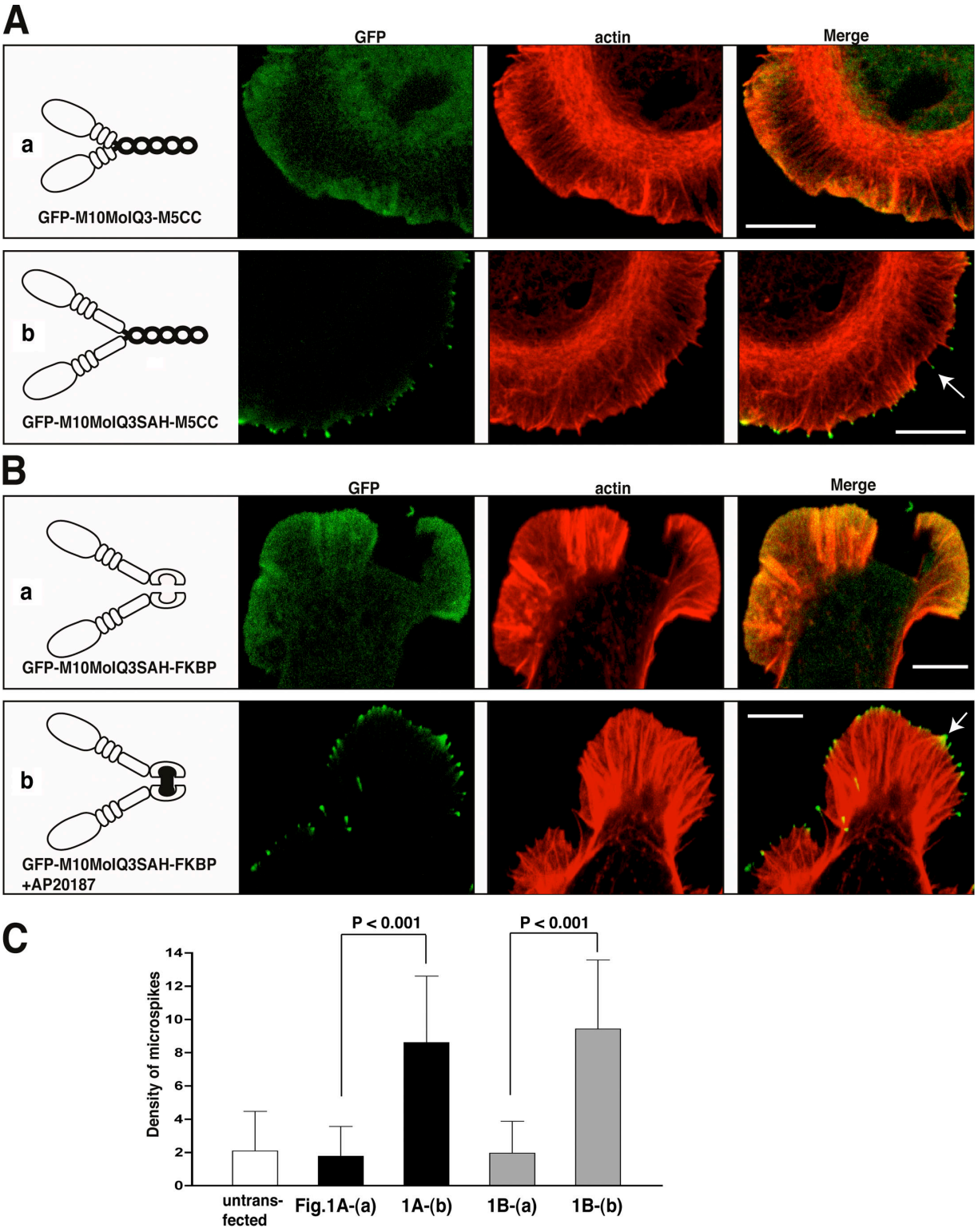

Figure 1. **Dimerization with proper neck length of myoX is critical for filopodia formation.** (A) Localization of the tailless myoX constructs franked with the coiled-coil domain of myoV. COS7 cells were transfected with GFP-M10MoIQ3-M5CC (a) or GFP-M10MoIQ3SAH-M5CC (b) and stained with rhodamine-phalloidin (red). Arrow indicates GFP-M10MoIQ3SAH-M5CC at the tip of filopodium. (B) The myoX constructs with the homodimerization domain induced filopodia formation upon addition of the dimerizer. NIH3T3 cells were transfected with GFP-M10MoIQ3SAH-FKBP (green) and replated on FN for 3 h with 100 nM AP20187. Red indicates rhodamine-phalloidin staining. Arrow indicates GFP-M10MoIQ3SAH-FKBP at the tip of filopodium. (C) Quantification of microspikes/filopodia. Microspikes/filopodia per 20 μm of the cell leading edge were counted in COS7 cells untransfected or transfected with the indicated constructs. The frequency of microspikes/filopodia was increased significantly by the addition of an SAH domain to M10MoIQ3 or forced dimerization with the SAH domain ($P < 0.001$). Error bars represent the mean ± SD. Bars, 10 μm.

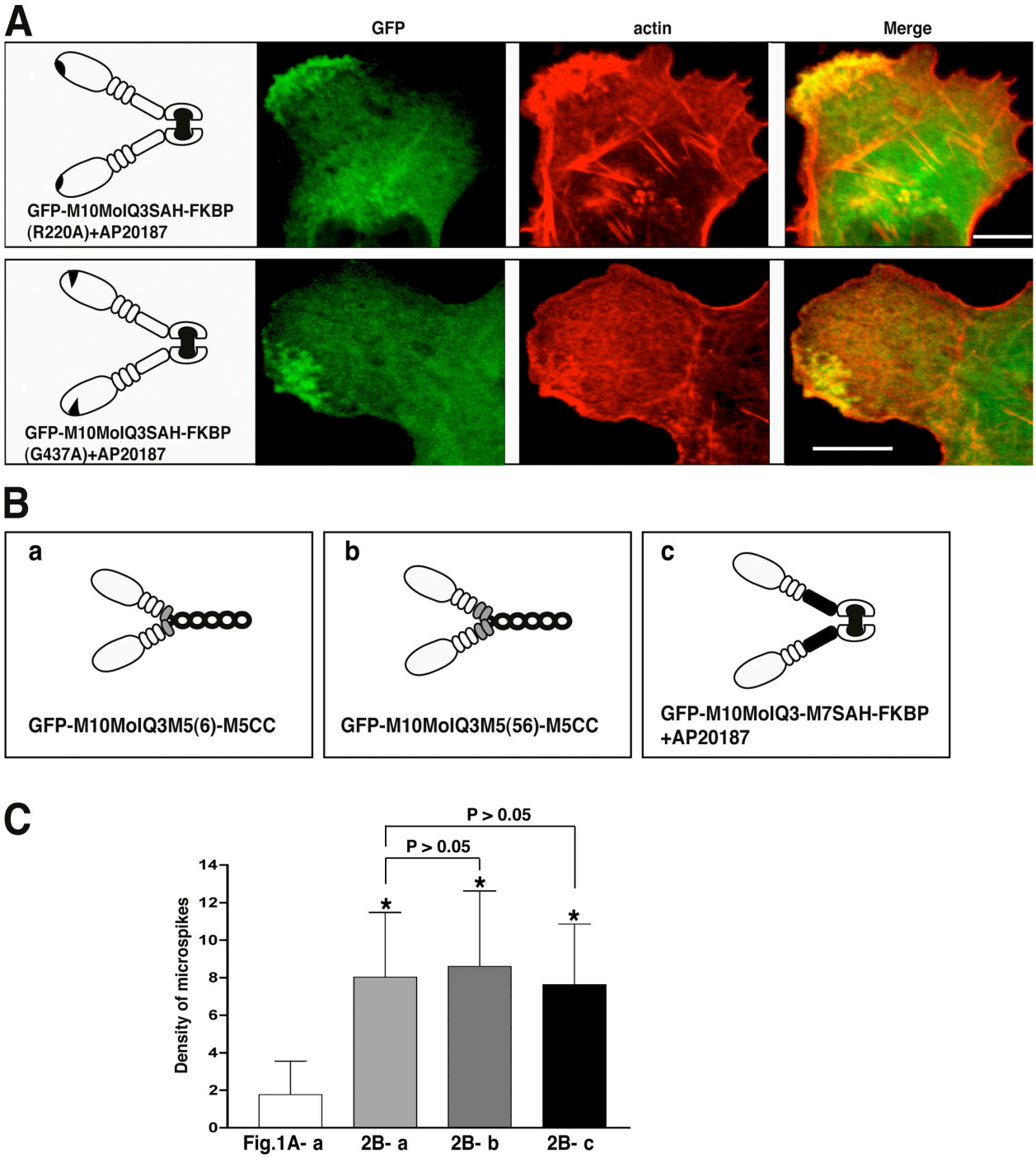

Figure 2. **The motor activity and neck length of myoX is essential for filopodia initiation.** (A) Localization of two different kinds of motor-dead myoX constructs of GFP-M10MoIQ3SAH-FKBP. COS7 cells were transfected with R220A mutant (top) or G437A mutant (bottom) and stained with rhodamine-phalloidin (red). (B) Schematic showing GFP-tagged constructs with different neck domains. (C) Quantification of microspikes/filopodia. Microspikes/filopodia were counted as described in Fig. 1. The frequency of microspikes/filopodia was increased significantly by the addition of one or two IQ domains of myoV to M10MoIQ3-M5CC or forced dimerization with myoVII's SAH domain. Error bars represent the mean ± SD. The asterisk indicates a significant difference ($P < 0.001$) in comparison with cells expressing GFP-M10MoIQ3-M5CC (Fig. 1 A, a). Bars, 10 μm.

molecules were subjected to electron microscopic observation. Approximately 70% of the molecules of M10MoIQ3SAH-FKBP were two headed in the presence of AP20187, whereas all of the molecules were monomeric in the absence of AP20187 (Fig. 3 C). These results clearly show that AP20187 induces the two-headed structure of M10MoIQ3SAH-FKBP.

The tailless myoX induces filopodia upon dimerization in living cells

Using the induced dimerization technique described in Fig. 1 B, we examined whether the formation of the two-headed structure of myoX directly related to the initiation of filopodia in the living cells. The representative images of spreading cells

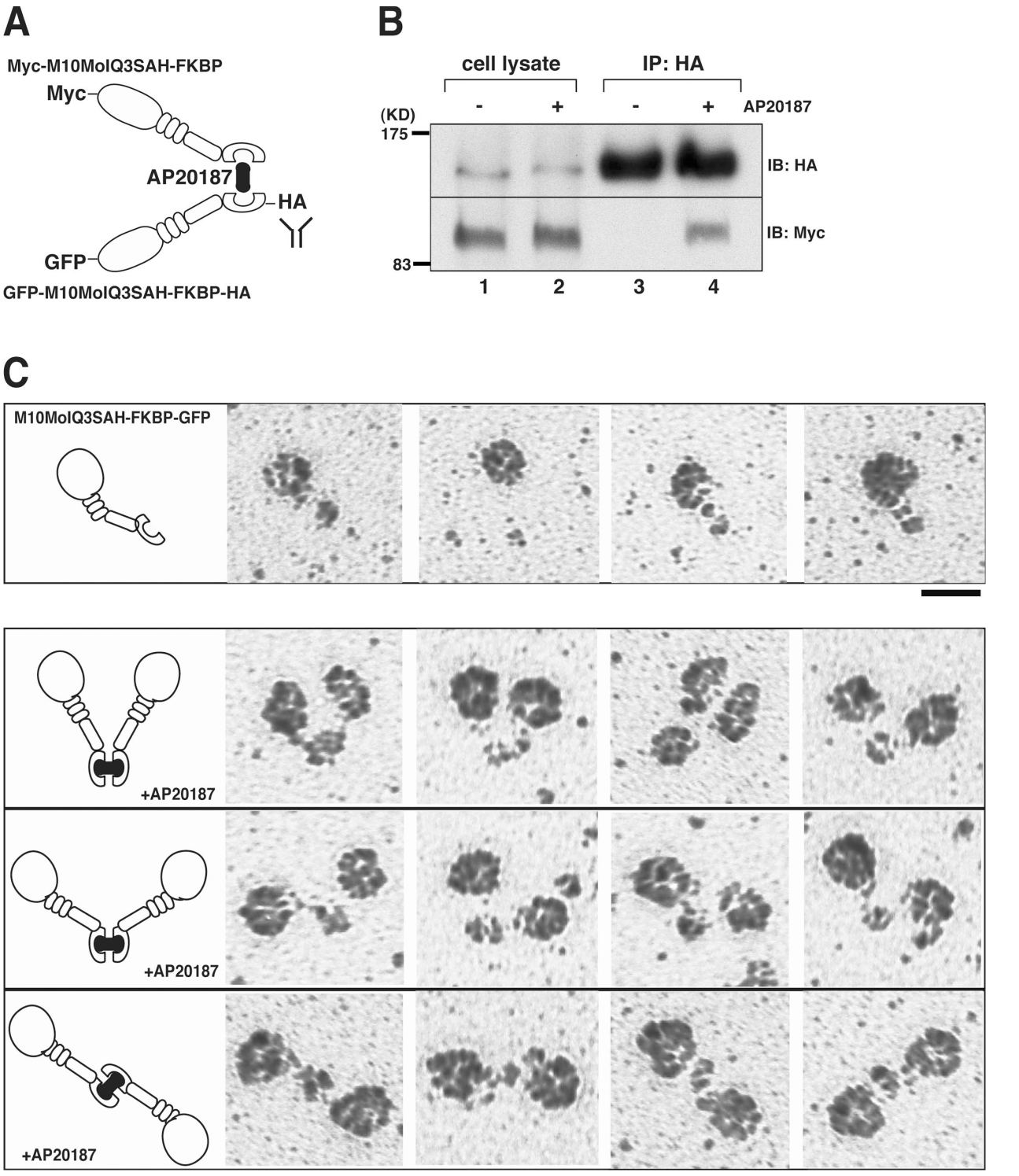

Figure 3. **The two-headed structure of myoX is induced by dimerizer.** (A) Schematic drawing of the dimerization of myc-M10MoIQ3SAH-FKBP with GFP-M10MoIQ3SAH-FKBP-HA induced by the dimerizing agent AP20187. (B) Dimer formation of myoX revealed by Western blot analysis. The experiment was performed as described in Materials and methods. (C) The rotary shadowing images of the one-headed and two-headed tailless myoX. (top) M10MoIQ3SAH-FKBP-GFP purified from the cells without AP20187. (bottom) M10MoIQ3SAH-FKBP-GFP purified from the cells in the presence of AP20187. The galleries illustrate the range of appearances of double-headed molecules showing the narrow-opened parallel (top) dimers, the wide-opened parallel (middle) dimers, and the antiparallel dimers (bottom). Bar, 5 nm.

plated on the fibronectin (FN)-coated coverslip are shown in Fig. 4 A and Video 1 (available at http://www.jcb.org/cgi/content/full/jcb.200703178/DC1). Before the addition of the dimerizer, GFP-M10MoIQ3SAH-FKBP showed diffuse localization throughout the cytosol, and fewer than three of the fluorescent puncta (the tip of filopodia) per cell appeared from the cell periphery

(Fig. 4 A, arrowhead). After the addition of the dimerizer, >20 additional fluorescent puncta appeared within 7 min (Fig. 4 A, bottom). Note that the induced new filopodia were produced only from the active ruffling area and quickly retracted to the edge (Video 1).

Fig. 4 B and Video 2 (available at http://www.jcb.org/cgi/content/full/jcb.200703178/DC1) show representative images of the migrating cells on the FN-coated coverslip. The cell shown in Fig. 4 B and Video 2 was observed migrating from the bottom to the top of the frame (Fig. 4 B, arrow). Before the addition of AP20187 (Fig. 4 B, top), substantial accumulation of GFP-M10MoIQ3SAH-FKBP at the leading edge was observed, and the predominant structure of the leading edge was lamellipodia. Approximately 3 min after the addition of AP20187, several short filopodia appeared from the leading edge and elongated in the direction of the migration (Fig. 4 B, bottom). However, the short filopodia retracted quickly to the edge of lamellipodia. The protrusion and retraction of the filopodia continued while the cell was moving forward. It should be noted that newly produced filopodia only protruded from the leading edge but never appeared from the lateral or the rear side of the migrating cells (Video 2). In contrast, AP21967 had no inducible effect on the production of filopodia (unpublished data).

It was also discovered that after the addition of AP20187, GFP-M10MoIQ3SAH-FKBP moved laterally along the leading edge and fused with another tip of filopodia (Fig. 4 C and Video 3, available at http://www.jcb.org/cgi/content/full/jcb.200703178/DC1). It should be emphasized that the lateral movement was not observed before addition of the dimerizer. Lateral movement of the full-length myoX has been reported using another cell line (Sousa et al., 2006). The present results suggest that the tail domain is not necessary for the lateral movement of myoX along the leading edge of lamellipodia and that formation of the two-headed structure is critical not only for intrafilopodial movement but also for lateral movement at the leading edge.

Knockdown of the expression of myoX

To further clarify the function of myoX in filopodia formation, experiments were conducted to eliminate the expression of endogenous myoX, and the effect of the deletion of myoX in actin dynamics was examined. The myoX-specific siRNA markedly reduced the expression of myoX as revealed by both Western blotting (Fig. S1 A) and immunocytochemistry (Fig. S1 B, available at http://www.jcb.org/cgi/content/full/jcb.200703178/DC1). In control double-stranded RNA–treated cells, the endogenous myoX localized at the tips of detectable actin filaments (bundles) that are aligned radially at the leading edge in lamellipodium. The elimination of myoX abolished not only the myoX localization at the tip of lamellipodia but also the radial arrangement of actin bundles at the cell periphery (Fig. S1 B). We also used pSIREN-DNR-DsRed plasmid that coexpresses small hairpin RNA (shRNA) and DsRed simultaneously to monitor the transfected cells. Two target sequences were used as a control: mouse specific (siM10m) and human specific (siM10h; Fig. S1 C). 3 d after the transfection, immunostaining showed that the expression of siM10m but not siM10h shRNAs markedly decreased levels of myoX in mouse NIH3T3 cells (Fig. S1 D). It should be noted that siM10m showed an effect on the actin structure similar to myoX-specific siRNA (Fig. 5 A).

To evaluate the specificity of the myoX knockdown phenotype, we performed rescue experiments. GFP-tagged bovine myoX (GFP-M10MoIQ3SAH-FKBP) that is refractory to siM10m shRNA restored microspike formation in cells expressing siM10m shRNA after the addition of AP20187 (Fig. 5, A and B; rescue). On the other hand, GFP-M10F also restored the formation of protrusion from lamellipodium. However, actin bundles were elongated to the long filopodia (unpublished data), which is consistent with a previous study showing that the full-length myoX induces long, stable filopodia (Berg and Cheney, 2002). These results indicate that the siRNA effect is specific to the loss of myoX but not as a result of off-target silencing. These results support the idea that myoX is important for promoting filopodia initiation in lamellipodia.

Based on these results, we propose the following model (Fig. 5 C). (1) MyoX is present as a dimer and monomer in the cells. The monomeric (single headed) myoX does not localize at the edge of lamellipodia. (2) Once the dimer is produced, myoX moves to the tip of the actin filaments, presumably as a result of its ability to walk on the actin filaments toward the barbed end. (3) The tips move laterally along the leading edge with actin filaments, and the mechanical activity of myoX plays a role in this process. (4) The lateral movement of myoX convergences on the barbed end of the actin filaments, thus producing the base of filopodia where the actin polymerization system might gather to induce parallel actin bundles.

According to the convergent elongation model of filopodia formation, the initiation step of filopodia consists of actin filament convergence and the barbed-end interaction in lamellipodia (Svitkina et al., 2003). We think that the lateral movement of dimerized myoX powers these movements and the structural changes of actin cytoskeleton in the lamellipodia. The function of the SAH domain can be related to the step size of myoX or the flexibility of the neck domain to search for an appropriate binding site on an actin protofilament. It has been reported that the shortening of the neck length of myoV markedly diminishes the run length (Purcell et al., 2002). Because the neck length (the number of IQ motifs) of myoX is one half of myoV, it is thought that the SAH domain functions to help myoX to find the proper actin monomer in the filament, thus facilitating the continuous movement.

Although the tailless myoX can initiate filopodia formation, the filopodia produced are short and unstable. These results suggest that the tail portion of myoX is important for the elongation and stabilization of filopodia and that these processes are likely to be controlled by the cargo molecules binding to the tail of myoX. Recently, it was reported that the unconventional myosin myosin-VI is dimerized after binding to Disabled-2 or the lipids phosphatidylinositol 4,5-disphosphate (Spudich et al., 2006). The pleckstrin homology domain of myoX also binds to the lipid phosphatidylinositol 3,4,5-trisphosphate in vitro (Tacon et al., 2004). Thus, it is possible that the dimer formation of myoX is induced by lipid binding. The tail domains of myoX

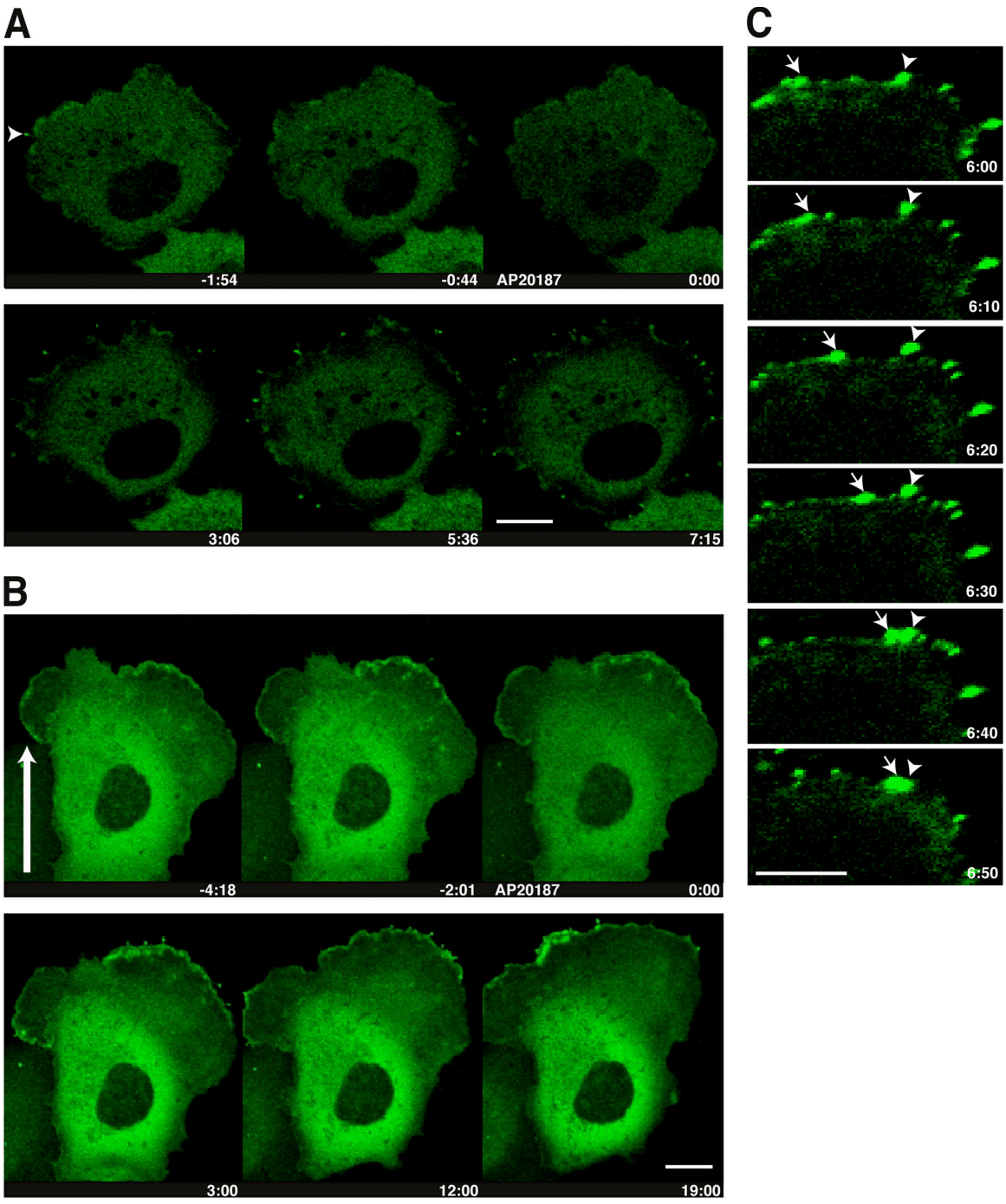

Figure 4. **The tailless myoX induces filopodia in the lamellipodia upon dimerization.** Time-lapse imaging shows the movement of GFP-M10MoIQ3SAH-FKBP in living COS7 cells. The numbers on the images indicate time (minutes/seconds) after the addition of 100 nM AP20187 to the culture medium. In the spreading cell (A) and in the migrating cell (B), GFP shows the localization of M10MoIQ3SAH-FKBP. The arrowhead in A shows that a filopodium existed before the addition of dimerizer. The arrow in B shows the moving direction of the cell. (C) Some fluorescent puncta (arrows) move laterally along the leading edge and fuse with another tip of filopodia (arrowheads). Bars (A and B), 10 μm; (C) 5 μm.

have binding partners such as microtubules (Weber et al., 2004), integrins (Zhang et al., 2004), and VASP (vasodilator-stimulated phosphoprotein; Tokuo and Ikebe, 2004). It is plausible that these binding proteins also control the dimer formation of myoX. Understanding the spatio-temporal regulation of the monomer-dimer transition of myoX in cells is a critical problem requiring further study.

Materials and methods

Plasmid construction

The construction of expression vector GFP-M10F was described previously (Tokuo and Ikebe, 2004). The cDNA encoding the first 811 amino acids, including the motor domain and the three IQ motifs, was amplified by PCR and subcloned in frame to pEGFP-C1 (pEGFP-M10MoIQ3). Inclusion of the SAH domain (the first 861 amino acids) was also constructed using the same method (pEGFP-M10MoIQ3SAH). The sequence of the coiled-coil

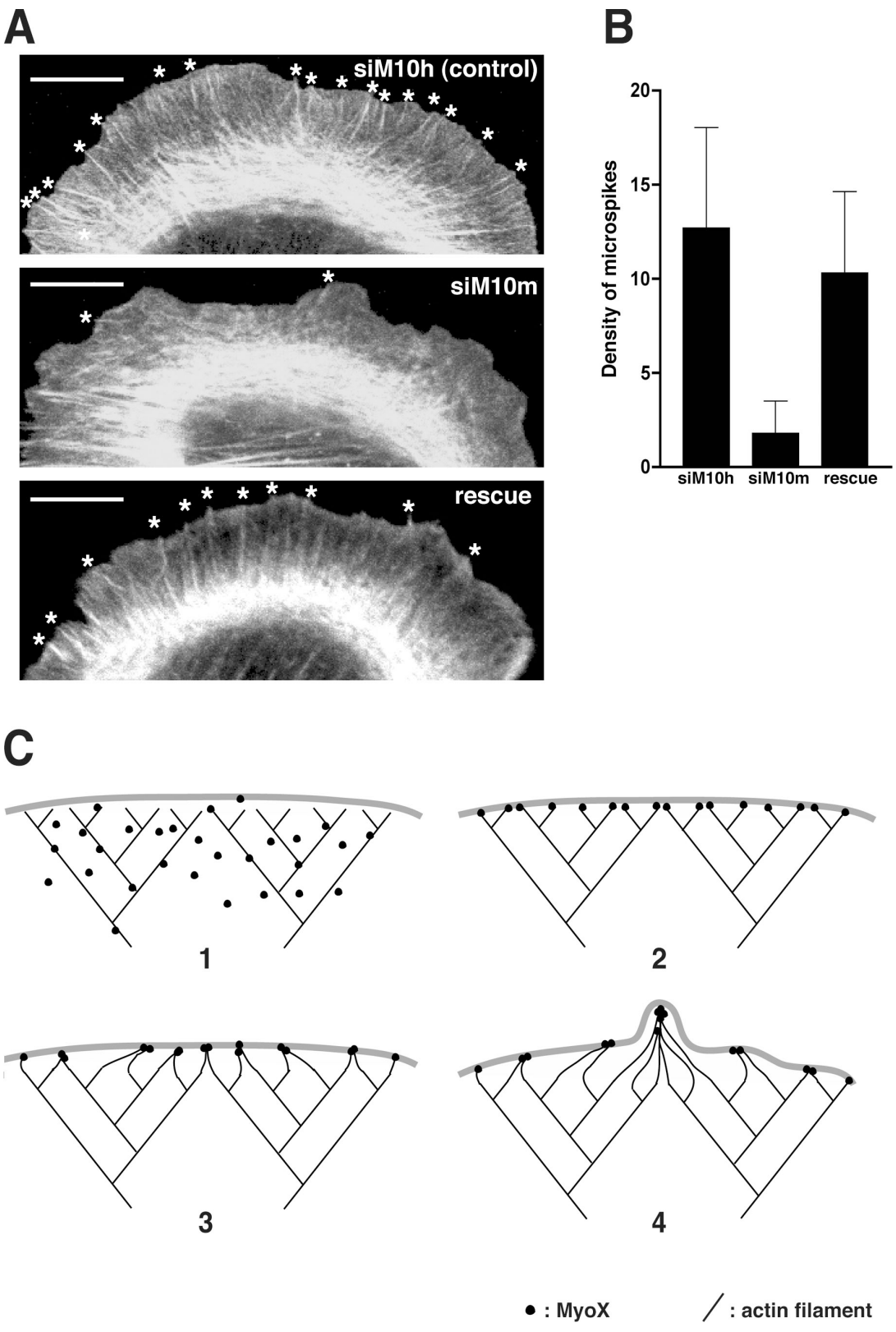

Figure 5. **MyoX is essential for filopodia induction from lamellipodia.** (A) Rescue of the knockdown phenotype by myoX. Fewer filopodia are seen in cells transfected with the knockdown construct (siM10m) compared with the control (siM10h). A cell expressing both siM10m shRNA and GFP-M10MoIQ3-SAH-FKBP (rescue) displays numerous microspikes after the addition of 100 nM AP20187. Asterisks show microspikes/filopodia. (B) Quantification of microspikes/filopodia. Microspikes/filopodia in NIH3T3 cells transfected with the indicated constructs were counted as described in Fig. 1. The frequency of microspikes/filopodia was decreased significantly by transfection with knockdown construct ($P < 0.001$). Error bars represent the mean ± SD. (C) Model of filopodia initiation upon the formation of the two-headed myoX. (1) MyoX is present as both a dimer and a monomer in the cells. The monomeric (single headed) myoX is present throughout the cytosol. (2) Once myoX forms the two-headed structure, myoX moves to the tips of the actin filaments, presumably

region of mouse myoV (M5CC; 907–1,090 amino acids) was amplified by PCR and fused to the aforementioned expression vectors (pEGFP-M10MoIQ3-M5CC and pEGFP-M10MoIQ3SAH-M5CC). Using the same methods, IQ6 to the coiled-coil region (885–1,090 amino acids) or IQ5 to the coiled-coil region (863–1,090 amino acids) was fused to pEGFP-M10MoIQ3 to create pEGFP-M10MoIQ3-M5(6)-M5CC and pEGFP-M10MoIQ3-M5(56)-M5CC, respectively.

Regulated dimerization system

Based on human FKBP and its small molecular ligands (Mallet et al., 2002), an FKBP was fused to the C-terminal end of the SAH domain of myoX (GFP-M10MoIQ3SAH-FKBP). The membrane-permeable drug created by chemical cross-linking of the two monomeric ligands with short linker (AP20187) can specifically bind to FKBP. If two FKBPs are present, AP20187 binds to both FKBPs, thus creating a dimer of the targeting molecule. As a control, we used AP21967, a chemically modified derivative of rapamycin that can induce the heterodimerization of FKBP and FRB-containing fusion proteins. To create pEGFP-M10MoIQ3-FKBP and pEGFP-M10MoIQ3SAH-FKBP, a fragment encoding FKBP was isolated from pC4-Fv1E (provided by ARIAD Pharmaceuticals) by restriction digestion and subcloned into pEGFP-M10MoIQ3 and pEGFP-M10MoIQ3SAH. pEGFP-M10MoIQ3-M7SAH-FKBP was created by swapping M10SAH for the rat myoVII SAH domain (M7SAH; 869–926 amino acids).

To determine the dimer formation by AP20187, COS7 cells were cotransfected with myc-M10MoIQ3SAH-FKBP and GFP-M10MoIQ3SAH-FKBP-HA. 16 h after transfection, 100 nM AP20187 was added to the culture medium and incubated for 30 min. The cell lysates were subjected to immunoprecipitation with anti-HA antibody. The immunoprecipitated samples were subjected to SDS-PAGE followed by Western blotting with anti-HA and anti-myc antibodies.

Motor-dead construct

The sequence of the switch I loop (NNNSSRFG; residues 215–220) of myoX with the exception of the second N is conserved in all nearby myosins sequenced so far (Shimada et al., 1997). The R to A mutation in the switch I loop results in loss of the ATP binding ability of skeletal myosin-II (Li et al., 1998) and the actin filament sliding activity of *Dictyostelium discoideum* myosin-II in the in vitro motility assay (Shimada et al., 1997). The motor domain of myoX also has a conserved sequence of the switch II loop (DIFGFE; residues 434–439) that has a charge interaction with switch I loop. This interaction is critical for ATP hydrolysis by myosin (Li et al., 1998). Although the G to A mutation in switch II does not abolish ATP binding to the active site, it causes the loss of ATP hydrolysis (Kambara et al., 1999) and actin sliding activity (Sasaki et al., 1998). According to the aforementioned results, we made two types of motor-dead constructs having a mutation in switch I (R220A) or in switch II (G437A) by site-directed mutagenesis (Kunkel, 1985, 1987) of pEGFP-M10MoIQ3SAH-FKBP (Fig. 2 A).

Cell culture and transfection

African green monkey kidney COS7 cells and NIH3T3 fibroblasts (American Type Culture Collection) were cultured in DME supplemented with 10% FCS. Transient transfections were performed with Fugene-6 (Roche Biochemicals) or LipofectAMINE 2000 (Invitrogen) according to the manufacturer's instructions. At 16 h after transfection, cells were trypsinized and replated on FN for 3 h, fixed, and stained with rhodamine-phalloidin.

Immunofluorescence microscopy

Immunofluorescence microscopy was performed as described previously (Tokuo and Ikebe, 2004). In brief, cells were cultured on 10 μg/ml FN-coated coverslips fixed with 4% formaldehyde, 2 mM $MgCl_2$, and 1 mM EGTA in PBS for 10 min at RT, treated with 0.2% Triton X-100 in PBS for 5 min, and washed with PBS. Blocking was performed by incubating the fixed cells with 5% BSA in PBS for 60 min at RT. After the antibodies had been diluted with the blocking solution, the cells were incubated at 4°C overnight with the primary antibody and subsequently for 30 min with the secondary antibody. For actin staining, AlexaFluor phalloidin (Invitrogen) was added to the secondary antibody. Specimens were observed at RT using a laser-scanning confocal microscope (DM IRB; Leica) controlled by a confocal microscope system (TCS SP II; Leica) equipped with a Plan-Apochromat 60× 1.40 NA oil immersion objective (Leica) with appropriate binning of pixels and exposure time. The images were processed using Photoshop 7.0 software (Adobe). Immunofluorescence video microscopy was imaged using the same system of immunofluorescence to control illumination shutters and camera exposure (Leica). Time-lapse images were obtained by sequential epifluorescent and phase illumination. The intervals were 10 s, and exposure times were 100–300 ms depending on the time-lapse interval and level of fluorescence. Cells were imaged over periods of 1–30 min at room temperature (25–30°C). Video files were created using QuickTime (Apple).

Quantification of microspikes/filopodia

Spread cells containing prominent lamella with leading edges were chosen from phalloidin-stained samples. The number of actin bundles touching (microspike) or crossing (filopodium) the edge was counted. Only bundles that have fluorescence intensity of at least 1.2 times above the background were considered. Data were analyzed using a *t* test. 50 cells (Figs. 1 C and 2 C) and 20 cells (Fig. 5 B) were quantified for each sample. For the rescue experiments, analysis of the number of microspikes/filopodia used cells expressing GFP-M10MoIQ3SAH-FKBP.

Immunoprecipitation and Western blotting analysis

Cells were lysed in lysis buffer (20 mM Hepes, pH 7.4, 150 mM NaCl, 2 mM $MgCl_2$, 0.2 mM EGTA, 1 mM ATP, 0.5% NP-40, 1 mM PMSF, 10 μg/ml leupeptin, 2 μg/ml pepstatin A, and 1 μg/ml trypsin inhibitor). The samples were centrifuged at 10,000 *g* for 20 min at 4°C, and the supernatants were incubated with antibodies conjugated to Affi-Prep Protein A (Bio-Rad Laboratories) for 2 h at 4°C. The precipitates were washed five times in ice-cold lysis buffer. The precipitates were dissolved in 5% SDS and 0.5 M $NaHCO_3$ buffer. These samples were then subjected to Western blotting as described previously (Tokuo and Ikebe, 2004).

Recombinant protein and electron microscopy

M10-MoIQ3SAH-FKBP-GFP was subcloned into pFastBac-HT baculovirus transfer vector (Invitrogen) containing a hexa-His-tag. The recombinant M10-MoIQ3SAH-FKBP-GFP protein was copurified with calmodulin as reported previously (Homma and Ikebe, 2005) with an additional incubation with or without 100 nM AP20187 (ARIAD Pharmaceuticals) for 30 min at RT before the cell lysis step. Rotary metal-shadowing electron microscopy of M10-MoIQ3SAH-FKBP-GFP was performed as described previously (Li et al., 2006). In brief, myoX proteins diluted to ~4 nM were absorbed onto a freshly cleaved mica surface for 30 s. Unbound proteins were rinsed away, and the specimen was stabilized by brief exposure to uranyl acetate as described previously (Mabuchi, 1990). The specimen was visualized by the rotary shadowing technique according to a previously described method (Mabuchi, 1991) with an electron microscope (model 300; Philips) at 60 kV.

siRNA experiments

The mouse myoX Stealth siRNA (target sequence 5′-GGAUGUCGGGCUGAUUGAUUCUGUA-3′ corresponding to nt 4,011–4,035 relative to the start codon) was generated by Invitrogen. Control siRNA was purchased from Dharmacon. pSIREN-DNR-DsRed-si*M10h* and -si*M10m* were constructed according to the manufacturer's instructions (BD Biosciences). The selected target sequences for si*M10h* was nt 135–153 of human myoX (GenBank/EMBL/DDBJ accession no. AF_234532) and for si*M10m* was nt 135–153 of mouse myoX (GenBank/EMBL/DDBJ accession no. NM_019472). si*M10h* and si*M10m* had three base mismatches; thus, si*M10h* served as a negative control of si*M10m*. The rescue construct (GFP-M10MoIQ3-SAH-FKBP) made from bovine myoX had four base mismatches to si*M10m* and were refractory to si*M10m* siRNA. The siRNA and plasmid transfection were performed using LipofectAMINE 2000 (Invitrogen) according to the manufacturer's instructions. The cells were analyzed 3 d after transfection.

Online supplemental material

Fig. S1 shows the depletion of myoX in NIH3T3 cells. Video 1 shows the movement of tailless myoX (GFP-M10-MoIQ3SAH-FKBP) in a spreading COS7 cell. Video 2 shows the movement of tailless myoX in a migrating COS7 cell. Video 3 shows lateral movement of the tailless myoX along the leading edge of a migrating cell upon addition of the dimerizer. Online

as a result of its ability to walk on the actin filaments toward the barbed end. (3) The tips of the actin filaments move laterally along the leading edge, with the motor function of myoX playing a role in this process. (4) The lateral drift induces a convergence of the barbed ends of the actin filaments, thus inducing the formation of microspikes. Bars, 5 μm.

supplemental material is available at http//www.jcb.org/cgi/content/full/jcb.200703178/DC1.

We would like to thank Ariad Pharmaceuticals for providing the plasmid pC4-Fv1E encoding Phe36Val mutant FKBP, AP20187, and AP21967. We also thank Dr. R.A. Fenton (University of Massachusetts Medical School, Worcester, MA) for reading the manuscript.

This work was supported by National Institutes of Health grants AR048526, AR048898, and DC006103.

Submitted: 27 March 2007
Accepted: 22 September 2007

References

Bohil, A.B., B.W. Robertson, and R.E. Cheney. 2006. Myosin-X is a molecular motor that functions in filopodia formation. *Proc. Natl. Acad. Sci. USA*. 103:12411–12416.

Bennett, R.D., A.S. Mauer, and E.E. Strehler. 2007. Calmodulin-like protein increases filopodia-dependent cell motility via up-regulation of myosin-10. *J. Biol. Chem.* 282:3205–3212.

Bentley, D., and T.P. O'Connor. 1994. Cytoskeletal events in growth cone steering. *Curr. Opin. Neurobiol.* 4:43–48.

Berg, J.S., and R.E. Cheney. 2002. Myosin-X is an unconventional myosin that undergoes intrafilopodial motility. *Nat. Cell Biol.* 4:246–250.

Berg, J.S., B.H. Derfler, C.M. Pennisi, D.P. Corey, and R.E. Cheney. 2000. Myosin-X, a novel myosin with pleckstrin homology domains, associates with regions of dynamic actin. *J. Cell Sci.* 113:3439–3451.

Biyasheva, A., T. Svitkina, P. Kunda, B. Baum, and G. Borisy. 2004. Cascade pathway of filopodia formation downstream of SCAR. *J. Cell Sci.* 117:837–848.

Homma, K., and M. Ikebe. 2005. Myosin X is a high duty ratio motor. *J. Biol. Chem.* 280:29381–29391.

Kambara, T., T.E. Rhodes, R. Ikebe, M. Yamada, H.D. White, and M. Ikebe. 1999. Functional significance of the conserved residues in the flexible hinge region of the myosin motor domain. *J. Biol. Chem.* 274:16400–16406.

Knight, P.J., K. Thirumurugan, Y. Xu, F. Wang, A.P. Kalverda, W.F. Stafford III, J.R. Sellers, and M. Peckham. 2005. The predicted coiled-coil domain of myosin 10 forms a novel elongated domain that lengthens the head. *J. Biol. Chem.* 280:34702–34708.

Kunkel, T.A. 1985. Rapid and efficient site-specific mutagenesis without phenotypic selection. *Proc. Natl. Acad. Sci. USA*. 82:488–492.

Kunkel, T.A., J.D. Roberts, and R.A. Zakour. 1987. Rapid and efficient site-specific mutagenesis without phenotypic selection. *Methods Enzymol.* 154:367–382.

Lebrand, C., E.W. Dent, G.A. Strasser, L.M. Lanier, M. Krause, T.M. Svitkina, G.G. Borisy, and F.B. Gertler. 2004. Critical role of Ena/VASP proteins for filopodia formation in neurons and in function downstream of netrin-1. *Neuron.* 42:37–49.

Lewis, A.K., and P.C. Bridgman. 1992. Nerve growth cone lamellipodia contain two populations of actin filaments that differ in organization and polarity. *J. Cell Biol.* 119:1219–1243.

Li, X.D., T.E. Rhodes, R. Ikebe, T. Kambara, H.D. White, and M. Ikebe. 1998. Effects of mutations in the gamma-phosphate binding site of myosin on its motor function. *J. Biol. Chem.* 273:27404–27411.

Li, X.D., H.S. Jung, K. Mabuchi, R. Craig, and M. Ikebe. 2006. The globular tail domain of myosin Va functions as an inhibitor of the myosin Va motor. *J. Biol. Chem.* 281:21789–21798.

Mabuchi, K. 1990. Melting of myosin and tropomyosin: electron microscopic observations. *J. Struct. Biol.* 103:249–256.

Mabuchi, K. 1991. Heavy-meromyosin-decorated actin filaments: a simple method to preserve actin filaments for rotary shadowing. *J. Struct. Biol.* 107:22–28.

Mallet, V.O., C. Mitchell, J.E. Guidotti, P. Jaffray, M. Fabre, D. Spencer, D. Arnoult, A. Kahn, and H. Gilgenkrantz. 2002. Conditional cell ablation by tight control of caspase-3 dimerization in transgenic mice. *Nat. Biotechnol.* 20:1234–1239.

Nakagawa, H., H. Miki, M. Nozumi, T. Takenawa, S. Miyamoto, J. Wehland, and J.V. Small. 2003. IRSp53 is colocalised with WAVE2 at the tips of protruding lamellipodia and filopodia independently of Mena. *J. Cell Sci.* 116:2577–2583.

Park, H., B. Ramamurthy, M. Travaglia, D. Safer, L.Q. Chen, C. Franzini-Armstrong, P.R. Selvin, and H.L. Sweeney. 2006. Full-length myosin VI dimerizes and moves processively along actin filaments upon monomer clustering. *Mol. Cell*. 21:331–336.

Purcell, T.J., C. Morris, J.A. Spudich, and H.L. Sweeney. 2002. Role of the lever arm in the processive stepping of myosin V. *Proc. Natl. Acad. Sci. USA*. 99:14159–14164.

Ridley, A.J., M.A. Schwartz, K. Burridge, R.A. Firtel, M.H. Ginsberg, G. Borisy, J.T. Parsons, and A.R. Horwitz. 2003. Cell migration: integrating signals from front to back. *Science*. 302:1704–1709.

Sasaki, N., T. Shimada, and K. Sutoh. 1998. Mutational analysis of the switch II loop of *Dictyostelium* myosin II. *J. Biol. Chem.* 273:20334–20340.

Shimada, T., N. Sasaki, R. Ohkura, and K. Sutoh. 1997. Alanine scanning mutagenesis of the switch I region in the ATPase site of *Dictyostelium discoideum* myosin II. *Biochemistry*. 36:14037–14043.

Sousa, A.D., and R.E. Cheney. 2005. Myosin-X: a molecular motor at the cell's fingertips. *Trends Cell Biol.* 15:533–539.

Sousa, A.D., J.S. Berg, B.W. Robertson, R.B. Meeker, and R.E. Cheney. 2006. Myo10 in brain: developmental regulation, identification of a headless isoform and dynamics in neurons. *J. Cell Sci.* 119:184–194.

Spudich, G., M.V. Chibalina, J.S. Au, S.D. Arden, F. Buss, and J. Kendrick-Jones. 2006. Myosin VI targeting to clathrin-coated structures and dimerization is mediated by binding to Disabled-2 and PtdIns(4,5)P(2). *Nat. Cell Biol*. 9:176–183.

Svitkina, T.M., E.A. Bulanova, O.Y. Chaga, D.M. Vignjevic, S. Kojima, J.M. Vasiliev, and G.G. Borisy. 2003. Mechanism of filopodia initiation by reorganization of a dendritic network. *J. Cell Biol.* 160:409–421.

Tacon, D., P.J. Knight, and M. Peckham. 2004. Imaging myosin 10 in cells. *Biochem. Soc. Trans.* 32:689–693.

Tokuo, H., and M. Ikebe. 2004. Myosin X transports Mena/VASP to the tip of filopodia. *Biochem. Biophys. Res. Commun.* 319:214–220.

Veigel, C., F. Wang, M.L. Bartoo, J.R. Sellers, and J.E. Molloy. 2002. The gated gait of the processive molecular motor, myosin V. *Nat. Cell Biol.* 4:59–65.

Weber, K.L., A.M. Sokac, J.S. Berg, R.E. Cheney, and W.M. Bement. 2004. A microtubule-binding myosin required for nuclear anchoring and spindle assembly. *Nature*. 431:325–329.

Wicki, A., F. Lehembre, N. Wick, B. Hantusch, D. Kerjaschki, and G. Christofori. 2006. Tumor invasion in the absence of epithelial-mesenchymal transition: podoplanin-mediated remodeling of the actin cytoskeleton. *Cancer Cell*. 9:261–272.

Yildiz, A., J.N. Forkey, S.A. McKinney, T. Ha, Y.E. Goldman, and P.R. Selvin. 2003. Myosin V walks hand-over-hand: single fluorophore imaging with 1.5-nm localization. *Science*. 300:2061–2065.

Zhang, H., J.S. Berg, Z. Li, Y. Wang, P. Lang, A.D. Sousa, A. Bhaskar, R.E. Cheney, and S. Stromblad. 2004. Myosin-X provides a motor-based link between integrins and the cytoskeleton. *Nat. Cell Biol.* 6:523–531.

Zhu, X.J., C.Z. Wang, P.G. Dai, Y. Xie, N.N. Song, Y. Liu, Q.S. Du, L. Mei, Y.Q. Ding, and W.C. Xiong. 2007. Myosin X regulates netrin receptors and functions in axonal path-finding. *Nat. Cell Biol.* 9:184–192.